American Mineralogist, Volume 92, pages 1368–1373, 2007

Imaging of dioctahedral 2:1 layers by high-resolution transmission electron microscopy (HRTEM): Possibility of recording the dehydroxylate

TOSHIHIRO KOGURE*

Department of Earth and Planetary Science, Graduate School of Science, The University of Tokyo, 7-3-1 Hongo, Bunkyo-ku, Tokyo, 113-0033, Japan

ABSTRACT

High-resolution transmission electron microscopy (HRTEM) images of dioctahedral 2:1 phyllosilicates (muscovite, paragonite, pyrophyllite, etc.) acquired by intense electron radiation may not record the natural state but rather the dehydroxylate phase, e.g., $NaAl_2Si_3AlO_{11}$ in the case of paragonite, $NaAl_2Si_3AlO_{10}(OH)_2$. Intense electron radiation on paragonite changes its electron diffraction pattern by a small increase in cell edges and a considerable decrease of the β angle, which are consistent with dehydroxylation. Comparison between experimental and simulated HRTEM images also indicates that the experimental image contrast is in better agreement with that for the dehydroxylate structure than the natural state. Thus, special care is necessary when analyzing the structures of dioctahedral 2:1 phyllosilicates from their HRTEM images, e.g., positions of octahedral cations that were proposed to change by migration during the dehydroxylation process.

Keywords: Electron microscopy, dioctahedral 2:1 phyllosilicates, paragonite, electron diffraction, phase transition

INTRODUCTION

Some dioctahedral 2:1 phyllosilicates, e.g., illite and dioctahedral smectite, are fine-grained phases and the distribution of cations among the octahedral sites in these minerals is a controversial issue (e.g., Ylagan et al. 2002; Drits 2003; Zviagina et al. 2004; Sainz-Díaz et al. 2005; Drits et al. 2006). There are two kinds of octahedral sites (*cis*- and *trans*- sites) in a 2:1 layer, depending on the location of coordinating hydroxyls. In the ideal dioctahedral sheet, one third of the total octahedral sites are vacant. If these vacancies are at the *trans*-site (or one *cis*-site), the structure is called "*trans*-vacant" (or "*cis*-vacant") (Drits 2003). Single-crystal X-ray structure analyses of dioctahedral 2:1 phyllosilicates with sufficient crystal size for analyses (e.g., muscovite, paragonite, margarite, pyrophyllite) showed that they are *trans*-vacant (e.g., Jackson and West 1931; Lin and Bailey 1984; Takéuchi 1966; Lee and Guggenheim 1981). However, some montmorillonite and illite samples were interpreted as *cis*-vacant structures (e.g., Tsipursky and Drits 1984; Drits et al. 1993, 1995), although their grains are too minute such that occupancies at the octahedral sites cannot be determined directly.

High-resolution transmission electron microscopy (HRTEM) of mica, if the specimen is observed with the incident electron beam parallel to the layers, can analyze the layer stacking and the occupancy at the interlayer sites semi-quantitatively (Kogure and Murakami 1996; Kogure 1997; Banfield and Murakami 1998). Dioctahedral and trioctahedral 2:1 layers can be distinguished by the image contrast at the octahedral sheet (Kogure 2002). This technique may give insights to the *trans*- and *cis*-site occupancies in dioctahedral micas. Several illite specimens that were expected to contain *cis*-vacant 2:1 layers were investigated but image contrast indicated that the *cis*-vacant 2:1 layer is not present (details will be reported elsewhere). An interesting phenomenon occurred in the HRTEM investigation of paragonite, a Na-bearing dioctahedral mica. The recorded HRTEM contrast showed features that are inconsistent with the reported crystal structure of paragonite. The results and conclusions obtained here are essential for the proper interpretation of octahedral cation occupancies in the dioctahedral 2:1 phyllosilicates using HRTEM techniques.

* E-mail: kogure@eps.s.u-tokyo.ac.jp

SAMPLES AND METHODS

The paragonite specimen used is a colorless, large flake from Kabo, Oyamachi, Hyogo-Prefecture, Japan (Geological Survey of Japan, GSJ-M 16481). The reported composition and cell dimensions (Sekino et al. 1975) are $(Na_{1.006}K_{0.035}Ca_{0.031})(Al_{1.841}Fe^{3+}_{0.059}Mg_{0.006})(Si_{2.870}Al_{1.130})O_{10}(OH)_2$ and a = 5.140 (4), b = 8.909 (7), c = 19.357 (8) Å, β = 94.58 (1)°. The muscovite specimen used is a colorless, large plate from pegmatite in Yamanoo, Ibaraki-Prefecture, Japan. The composition and cell dimensions were not determined and typical values (e.g., Brigatti et al. 1998) were assumed.

Specimens for TEM examination were prepared by using the method in Kogure (2002). A cleaved plate was embedded with epoxy resin between two glass slides. After hardening, the glass slides were cut using a diamond wheel to laths of ~1 mm thickness. The laths were thinned to ~50 μm by mechanical grinding and then argon ion milled. HRTEM examination was performed at 200 kV using a JEOL JEM-2010. HRTEM images were recorded on films with magnification of ×400 000 or ×500 000. Selected images were digitized using a CCD camera for image processing. Noise from amorphous materials in HRTEM images was removed using Wiener-filter (Marks 1996; Kilaas 1998) developed by K. Ishizuka (HREM Research Inc.) and implemented with Gatan DigitalMicrograph version 3.10.0. A Gatan ES-500W CCD camera equipped at a port of the column just above the phosphor screen of the TEM was used to acquire diffraction patterns. For the accurate measurement of angles in HRTEM images or diffraction patterns, the images or patterns must be free from distortion. The distortion for the TEM used was estimated using HRTEM images and diffractions from silicon oriented

0003-004X/07/0809–1368$05.00/DOI: 10.2138/am.2007.2539

to the <110> direction. It was found that the image and diffraction were elongated (or shrunk) by about 3% along a certain direction. This distortion was corrected using Adobe PhotoShop.

Multi-slice image simulation was performed using MacTempas (Total Resolution Co.). Images were simulated using parameters for JEM-2010 electron microscope; viz. spherical aberration coefficient of 0.5 mm, spread of focus half width of 10 nm, beam convergence of 0.5 mrad, the objective aperture corresponded to 7.0 nm^{-1}, and acceleration voltage of 200 kV (the specimen thickness and defocus value are described in the captions for each figure).

Results

Figure 1 shows HRTEM images of muscovite and paragonite, recorded along [$\bar{1}$10]. Both images show a two-layer periodicity of the 2:1 layer, according to the 2M_1 polytype common in these micas. Paragonite shows a smaller d_{001} value (19.2 Å) than that (19.9 Å) of muscovite owing to a narrower interlayer accommodating Na ions. The contrast at the dioctahedral 2:1 layer is equal for both minerals, and the contrast is also identical to that for muscovite (Banfield and Murakami 1998) and pyrophyllite (Kogure et al. 2006). The contrast for *trans*-vacant dioctahedral 2:1 layers consists of dark spots at the tetrahedral sheets corresponding to a pair of tetrahedra (or tetrahedral chains passing along the electron-beam direction), and dark spots at the dioctahedral sheet correspond to a pair of *cis*-octahedra of Al separated by *trans*-vacant sites (see Fig. 3 in Kogure et al. 2006). If the intralayer shift (the lateral shift of about *a*/3 between the lower and upper tetrahedral sheets) in the 2:1 layer is parallel or anti-parallel to the beam direction, the three dark spots are aligned vertically in the layer. However, the three dark spots are obliquely aligned if the intralayer shift is 60 or 120° away from the beam direction (Kogure et al. 2006).

Although the basic feature of the images is expected from the crystal structures of muscovite and paragonite, the detail of the image from paragonite is problematic. The two lines that correspond to (001) and (110) planes are drawn by connecting the identical points and the subtended angle is 84.8 and 87.2° in muscovite and paragonite, respectively (Fig. 1). The expected value for muscovite is 84.9 to 85.0°, if typical cell dimensions are used. The discrepancy is within the error of measurement in the image (the maximum deviation is ~0.2° among ten measurements). In contrast, the expected value for paragonite is 86.2°, based on the cell dimensions for this specimen. The discrepancy of about 1.0° is significantly larger than the experimental error.

To determine whether the angle discrepancy is a result of a phase change that occurs during sample preparation or HRTEM observation, selected-area diffraction (SAD) patterns from paragonite were recorded before and after intense electron radiation similar to that experienced by a sample examined as in Figure 1. Figure 2 shows SAD patterns of paragonite along [$\bar{1}$10] (2a) before and (2b) after intense electron radiation. The near-horizontal line in Figure 2a connects the 00$\bar{3}$ and 33$\bar{3}$ reflections. The same line is drawn in Figure 2b. The line is slightly offset from the 33$\bar{3}$ reflection (arrow) in Figure 2b, suggesting that the small modification of the diffraction pattern was caused by electron radiation. Figure 3 shows measured change of the angle between 00*l* and 11*l* reflections and two *d*-values (d_{002} and d_{110}), which were measured from the SAD patterns as shown in Figure 2, as a function of radiation time of electron radiation (about 0.3 Å/cm^2 or 200 electron/s/$Å^2$ on the specimen). During the recording of the SAD pattern, the radiation intensity was decreased to less than one tenth.

In addition to a change in the angle between the lines connecting reflections, there is also a slight increase of the lattice spacing (*d*-value). In Figure 3, the absolute values for the lattice spacing are not accurate because the camera constant is not precisely calibrated. However, relative change of the values is significant because the recording conditions were fixed (e.g., currents of the lenses did not change).

Discussion

Variations of the cell dimensions in Figure 3 probably correspond to the dehydroxylation of paragonite. Dioctahedral 2:1 micas are known to dehydroxylate topotactically at elevated temperatures (e.g., Brigatti and Guggenheim 2002). Dehydroxylation and the dehydroxylate structure were reported for pyrophyllite (Wardle and Brindley 1972), muscovite (Udagawa et al. 1974), and paragonite (Comodi and Zanazzi 2000). The dehydroxylation

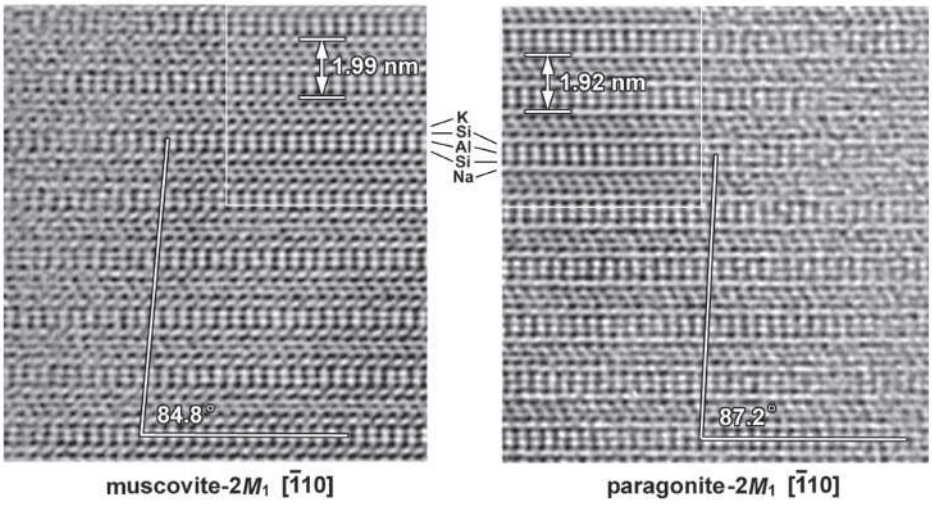

Figure 1. HRTEM images of muscovite-2M_1 (left) and paragonite-2M_1 (right), recorded along the [$\bar{1}$10] direction. The upper-right portion in muscovite and upper-left portion in paragonite are the Wiener-filtered images. The angles between the two lines that correspond to (001) and (110) are shown. From the crystallographic parameters, these angles are expected to be 84.9–85.0° for muscovite and 86.0° for paragonite. In contrast these values are 84.8 and 87.2° in the HRTEM images.

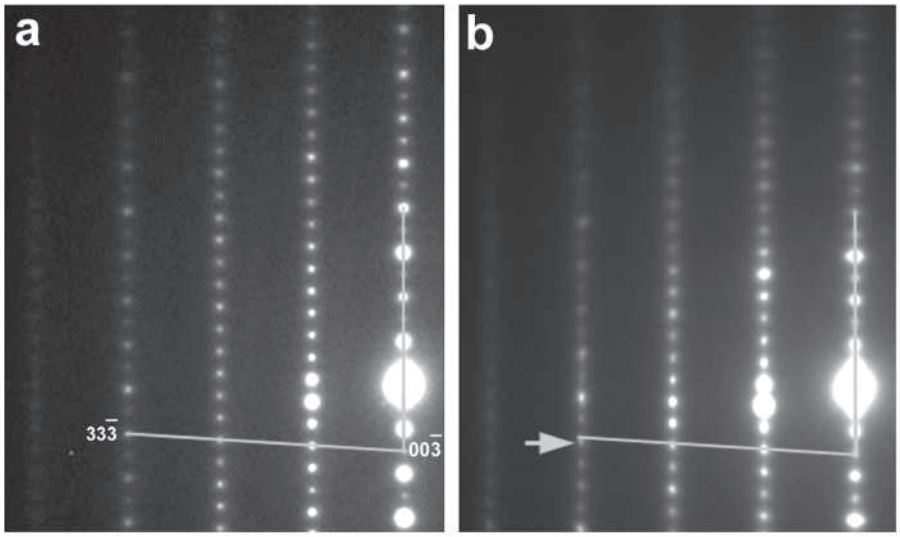

FIGURE 2. Selected area diffraction pattern from paragonite recorded along [$1\bar{1}0$] before and (**b**) after intense beam radiation. The near-horizontal lines in **a** and **b** are drawn from the $00\bar{3}$ reflection with the same angle from a line along the 00*l* reflections. Note that the line passes over the $33\bar{3}$ reflection in **a** but does not in **b**, as indicated by the arrow, suggesting that structural changes occur.

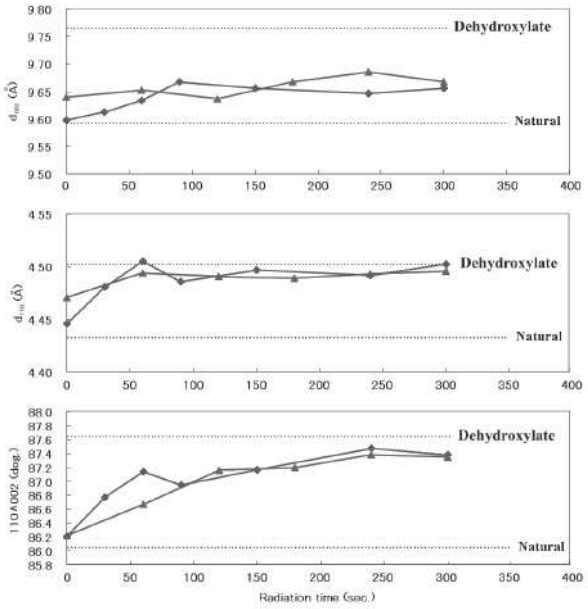

FIGURE 3. The change of d_{002}, d_{110}, and the angle between 110 and 002 reflections in the diffraction pattern during beam radiation. The beam current is about 0.3 Å/cm^2 on the specimen. The two solid lines in each graph represent different runs (see the text for discussion).

process of paragonite is expressed as $NaAl_2Si_3AlO_{10}(OH)_2 \rightarrow NaAl_2Si_3AlO_{11} + H_2O$. According to Comodi and Zanazzi (2000), dehydroxylation causes the edge lengths of the unit cell to increase by about 1% in *a* and *c*, and 2.4% in *b*. These changes are roughly similar also in the dehydroxylation of pyrophyllite and muscovite (Brigatti and Guggenheim 2002). The 2.4% increase of the *b* length is attributed to a change in configuration of the "octahedral" sheet with Al in fivefold coordination. The β angle decreases by ~2° in dehydroxylation of paragonite whereas the angle remains constant for muscovite. The variation in the β angle involves an increase of lateral dimension of the octahedral sheet by dehydroxylation. This increase in dimension causes a decrease of the ditrigonal rotation angle of the tetrahedral sheet to compensate for the mismatch between the tetrahedral and octahedral sheets. As shown by Kogure et al. (2005), a decrease of the ditrigonal rotation angle produces an increase of the cavity space in the tetrahedral sheet, which causes layer offset (the lateral shift between the two tetrahedral sheets across the interlayer region, Lin and Bailey 1984) in the case of Na-bearing mica. The driving force of the layer offset is repulsion between the two tetrahedral sheets facing each other across the interlayer, and the small ionic radius of Na relative to the cavity space. This layer offset (or interlayer displacement, Kogure et al. 2006) affects the β angle. In muscovite, the K ion is sufficiently large to interlock the two tetrahedral sheets with no layer offset, even if the cavity space is increased by dehydroxylation. The d_{002}, d_{110}, and the angle between 00*l* and 11*l* reflections, expected from the cell dimensions of paragonite and its dehydroxylate are given in Figure 3. The cell parameters for paragonite and its dehydroxylate in Figure 3 are from Sekino et al. (1975) and Comodi and Zanazzi (2000), respectively. The difference in cell parameters for natural paragonite between Sekino et al. (1975) and Comodi and Zanazzi (2000) is negligible, compared with differences between natural paragonite and its dehydroxylate. The variations in the experimental values for the angle and d_{110} are nearly explained by dehydroxylation, although the change of d_{002} is smaller than expected.

Figure 4 shows the experimental HRTEM contrast (Wiener-filtered) along the [$\bar{1}10$] direction, and those calculated from the crystal structures of natural and dehydroxylated paragonite (Comodi and Zanazzi 2000). Figure 5 is a projection of a polyhedral drawing of the two phases, viewed along the [$\bar{1}10$] direction. Careful comparison shows that the calculated contrast for the dehydroxylate matches the experimental image better than that for natural paragonite. Several features are noteworthy. First, the relative position between adjacent layers is well reproduced in the calculated image contrast for the dehydroxylate (cf. vertical white lines). This is related to the similar amount of stagger (i.e., the layer offset) at the interlayer (cf. slant of the short white bars in the three images). Secondly, the bright white spots within the

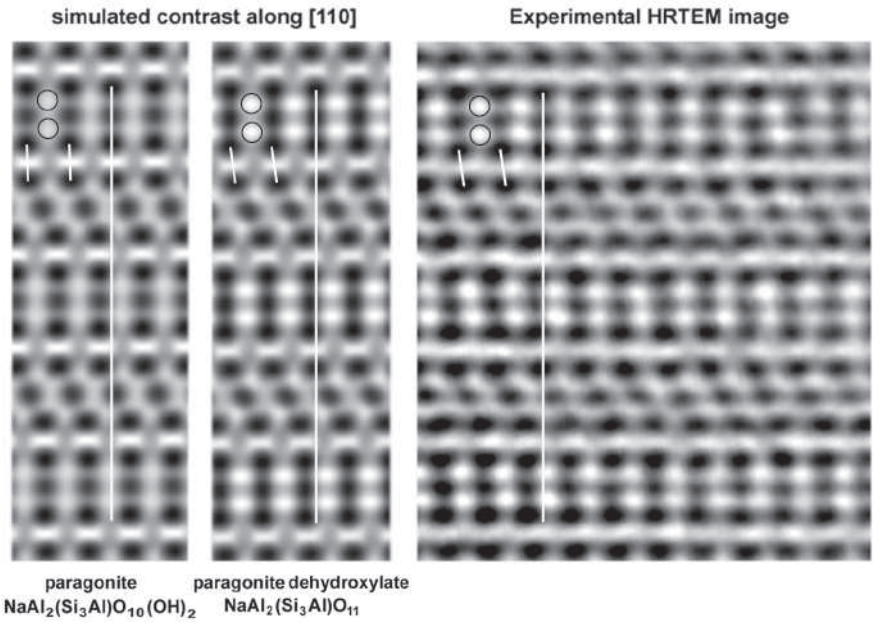

FIGURE 4. Experimental HRTEM image (Wiener-filtered) and simulated contrasts for paragonite and its dehydroxylate. The thickness and defocus value for the simulation are 2.5 nm and –40 nm, respectively. Note that the relative position between adjacent layers (cf. white vertical lines) in the experimental image is consistent with that in the dehydroxylated structure rather than the natural structure. This result is related to the lateral displacement between the two tetrahedral sheets across the interlayer, as shown by the slant of the short white bars connecting the dark spots. Note also that the white spots in the 2:1 layer (circles) in the experimental image are well reproduced in the contrast for the dehydroxylate structure.

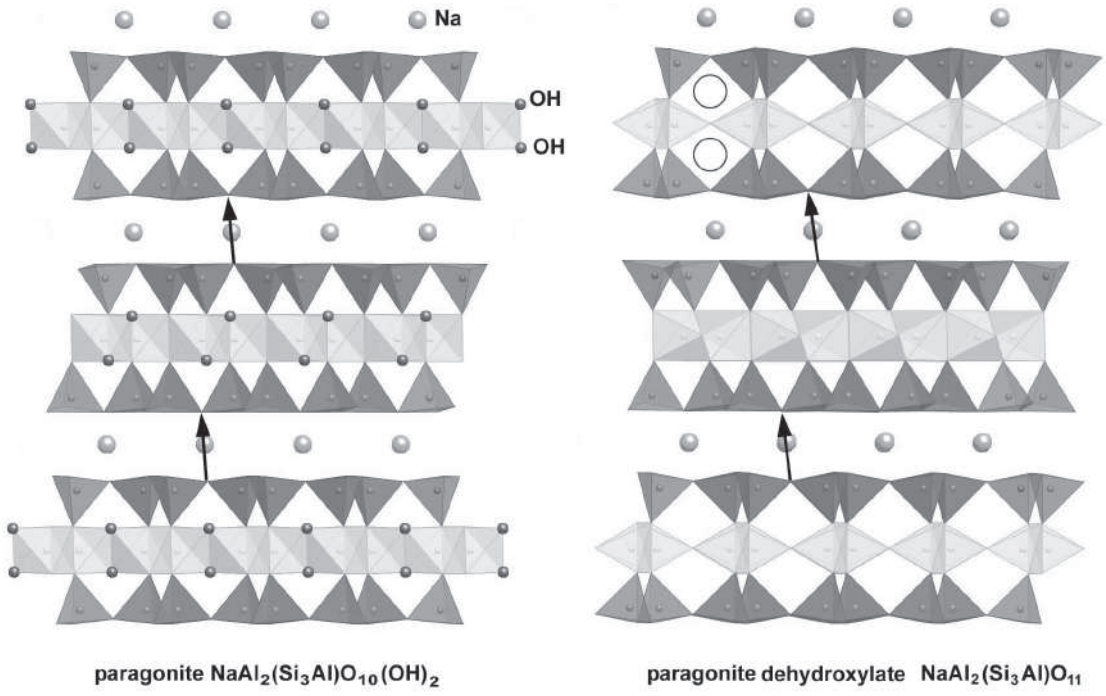

FIGURE 5. Polygonal drawing of the crystal structures of paragonite and its dehydroxylate viewed along [$\bar{1}$10], using the data of Comodi and Zanazzi (2000). The arrows in the interlayer connect the center of the hexagonal cavities in the two tetrahedral sheets across the interlayer. The circles at the top-left of the dehydroxylate structure indicate the channels formed by dehydroxylation, which correspond to the bright spots circled in the simulated contrast in Figure 4.

2:1 layer (circles) are distinct in the experimental image, when the intralayer shift is parallel to the viewing direction. This characteristic contrast is also well reproduced in the calculated image for the dehydroxylate. These bright spots correspond to the atomic channels in the dehydroxylated structure (Fig. 5). Two adjacent hydroxyls are liberated from the structure to form a H_2O molecule and residual oxygen atoms remain after heat treatment. These residual oxygen atoms reside in the same plane as the fivefold-coordinated cations in the dehydroxylate phase (Wardle and Brindley 1972) and the channels parallel to [$\bar{1}$10] or [110] are formed as shown in Figure 5. Figure 6 shows the result of further image simulation, changing the specimen thickness and defocus condition within the range where dark three spots at the 2:1 layer are distinctively observed. The bright white spots are

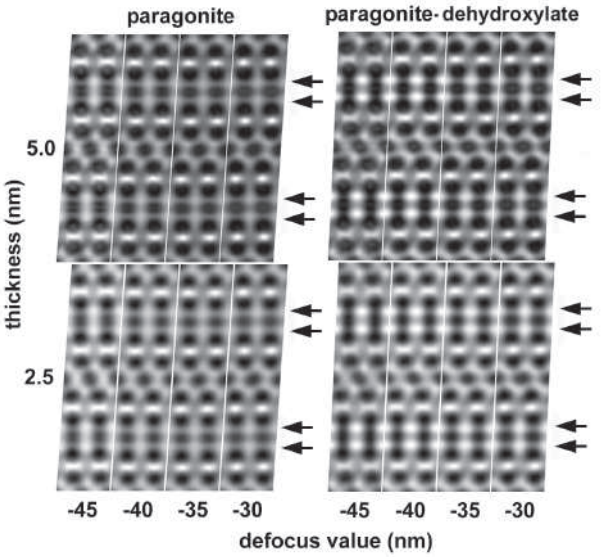

FIGURE 6. Multi-slice calculation of the contrasts for paragonite and its dehydroxylate projected along [$\bar{1}$10], as functions of the specimen thickness and defocus value. Note that the distinct white spots within the 2:1 layer (arrows) appear in a wider range of the thickness and defocus value in the dehydroxylate.

reproduced more commonly for the paragonite dehydroxylate phase than for paragonite.

From these results, the HRTEM images originally believed to be of paragonite in the present study are actually from the dehydroxylate phase. In the case of muscovite or pyrophyllite, the change of the β angle is more subtle and the relative position of adjacent layers is not altered by dehydroxylation. However, the distinctive bright spots in the 2:1 layer with the intralayer shift parallel to the beam direction are also observed in Figure 1a for muscovite and in Kogure et al. (2006) for pyrophyllite (cf. Figs. 3 and 4 in Kogure et al. 2006), indicating that dehydroxylation of the dioctahedral 2:1 layer by intense electron radiation is a common phenomenon. The dehydroxylation of the aluminous *trans*-vacant 2:1 layer by heat treatment starts at 500–550 °C in air (Udagawa et al. 1974; Wardle and Brindley 1972). It is unlikely that electron radiation increases the specimen temperature to 500 °C. However, dehydroxylation of hydrous minerals by beam radiation is a common phenomenon, e.g., goethite (FeOOH) to hematite (Fe_2O_3) (Van Landuyt et al. 1987), brucite [$Mg(OH)_2$] to periclase (MgO) (Dahmen et al. 1987), gibbsite [$Al(OH)_3$] to γ-alumina (Al_2O_3) (Kogure 1999). These dehydroxylated phases are topotactic to the original phases.

Two types of radiation damage generally can occur in TEM, knock-on damage and radiolytic damage. For silicates at the electron energy used here (200 keV), radiolytic damage, where the energy from the incident electron is transferred to the electrons in the specimen and where chemical bonds may be broken, is dominant (Csencsits and Gronsky 1987). The H_2O molecule is generated by the breakage of an O-H bond and the generated proton reacts with an adjacent hydroxyl, probably by electron radiation in TEM. In addition, the specimen is under vacuum and it is very thin. Generated H_2O molecules easily diffuse to the specimen surface and are desorbed into the vacuum.

In Figure 3, the change in cell dimensions occurs about one minute after intense electron radiation. This intensity (0.3 A/cm^2 on the specimen) is several times weaker than that required to record HRTEM images on film with a magnification of 400 000 to 500 000. Therefore, HRTEM recording before dehydroxylation is almost impossible or needs special care and quick operation.

These results are important for the interpretation of HRTEM images from dioctahedral 2:1 phyllosilicates. For instance, the migration of octahedral cations occurs in *cis*-vacant illite and montmorillonite, and in *trans*-vacant glauconite and celadonite during dehydroxylation (Drits et al. 1995; Muller et al. 2000a, 2000b). *Cis*-vacant illite transforms to *trans*-vacant by dehydroxylation at high temperature (Drits et al. 1995). Although not presented here, HRTEM data from several illite specimens that were expected to have *cis*-vacant 2:1 layers always showed a contrast interpreted to be *trans*-vacant. This is probably related to dehydroxylation by electron radiation in TEM.

ACKNOWLEDGMENTS

The author is greatful to Y. Banno (Geological Survey of Japan, AIST) for donating the paragonite specimen. He also thanks V.A. Drits (Russian Academy of Sciences), S. Guggenheim (University of Illinois at Chicago), and I. Dodony (Lorand Eotvos University, Hungary) for their comments on the manuscript. He is also grateful to T. Takeshige (the University of Tokyo) for preparation of the TEM specimens. Transmission electron microscopy was performed in the Electron Microbeam Analysis Facility of Department of Earth and Planetary Science, the University of Tokyo. This work was partly supported by a Grant-in-Aid no. 17340160 [Section (B)] by the Japan Society for the Promotion of Science (JSPS).

REFERENCES CITED

Banfield, J.F. and Murakami, T. (1998) Atomic-resolution transmission electron microscope evidence for the mechanism by which chlorite weathers to 1:1 semi-regular chlorite-vermiculite. American Mineralogist, 83, 348–357.

Brigatti, M.F. and Guggenheim, S. (2002) Mica crystal chemistry and the influence of pressure, temperature, and solid solution on atomistic models. In A. Mottana, F.P. Sassi, J.B. Thompson, Jr., S. Guggenheim, Eds., Micas: Crystal Chemistry and Metamorphic Petrology, 46, p. 1–98. Reviews in Mineralogy and Geochemistry, Mineralogical Society of America, Chantilly, Virginia.

Brigatti, M.F., Frigieri, P., and Poppi, L. (1998) Crystal chemistry of Mg-, Fe-bearing muscovites-2M_1. American Mineralogist, 83, 775–785.

Comodi, P. and Zanazzi, P.F. (2000) Structural thermal behaviour of paragonite and its dehydroxylate: a high-temperature single-crystal study. Physics and Chemistry of Minerals, 27, 377–385.

Csencsits, R. and Gronsky, R. (1987) Damage of zeolite Y in the TEM and its effects on TEM images. Ultramicroscopy, 23, 421–431.

Dahmen, U., Kim, M.G., and Searcy, A.W. (1987) Microstructural evolution during the decomposition of $Mg(OH)_2$. Ultramicroscopy, 23, 365–370.

Drits, V.A. (2003) Structural and chemical heterogeneity of layer silicates and clay minerals. Clay Minerals, 38, 403–432.

Drits, V.A., Weber, F., Salyn, A.L., and Tsipursky, S.I. (1993) X-ray identification of one-layer illite varieties: application to the study of illites around uranium deposits of Canada. Clays and Clay Minerals, 41, 389–398.

Drits, V.A., Besson, G., and Muller, F. (1995) An improved model for structural transformations of heat-treated aluminous dioctahedral 2:1 layer silicates. Clays and Clay Minerals, 43, 718–731.

Drits, V.A., McCarty, D.K., and Zviagina, B.B. (2006) Crystal-chemical factors responsible for the distribution of octahedral cations over *trans*- and *cis*-sites in dioctahedral 2:1 layer silicates. Clays and Clay Minerals, 54, 131–152.

Jackson, W.W. and West, J. (1931) The crystal structure of muscovite-$KAl_3Si_3O_{10}(OH)_2$. Zeitschrift für Kristallographie, 76, 211–277.

Kilaas, R. (1998) Optimal and near-optimal filters in high-resolution electron microscopy. Journal of Microscopy, 190, 45–51.

Kogure, T. (1997) On the structure of cleaved surfaces in biotite mica. Mineralogical Journal, 19, 155–164.

——— (1999) Dehydration sequence of gibbsite by electron-beam irradiation in a TEM. Journal of American Ceramic Society, 82, 716–720.

——— (2002) Investigation of micas using advanced TEM. In A. Mottana, F.P. Sassi, J.B. Thompson, Jr., S. Guggenheim, Eds., Micas: Crystal Chemistry and Metamorphic Petrology, 46, p. 281–312. Reviews in Mineralogy and Geochemistry, Mineralogical Society of America, Chantilly, Virginia.

Kogure, T. and Murakami, T. (1996) Direct identification of biotite/vermiculite

layers in hydrobiotite using high-resolution TEM. Mineralogical Journal, 18, 131–137.
Kogure, T., Miyawaki, R., and Banno, Y. (2005) The true structure of wonesite, an interlayer-deficient trioctahedral sodium mica. American Mineralogist, 90, 725–731.
Kogure, T., Jige, M., Kameda, J., Yamagishi, A., Miyawaki, R., and Kitagawa, R. (2006) Stacking structures in pyrophyllite revealed by high-resolution transmission electron microscopy (HRTEM). American Mineralogist, 91, 1293–1299.
Lee, J.H. and Guggenheim, S. (1981) Single crystal X-ray refinement of pyrophyllite-1*Tc*. American Mineralogist, 66, 350–357.
Lin, C.Y. and Bailey, S.W. (1984) The crystal structure of paragonite-2M_1. American Mineralogist, 69, 122–127.
Marks, L.D. (1996) Wiener-filter enhancement of noisy HREM images. Ultramicroscopy, 62, 43–52.
Muller, F., Drits, V.A., Plançon, A., and Besson, G. (2000a) Dehydroxylation of Fe^{3+}, Mg-rich dioctahedral micas: (I) structural transformation. Clay Minerals, 35, 491–504.
Muller, F., Drits, V.A., Tsipursky, S.I., and Plançon, A. (2000b) Dehydroxylation of Fe^{3+}, Mg-rich dioctahedral micas: (II) cation migration. Clay Minerals, 35, 505–514.
Sainz-Díaz, C.I., Escamilla-Roa, E., and Hernandez-Laguna, A. (2005) Quantum mechanical calculations of *trans*-vacant and *cis*-vacant polymorphism in dioctahedral 2:1 phyllosilicates. American Mineralogist, 90, 1827–1834.
Sekino, H., Kanisawa, S., Harada, K., and Ishikawa, Y. (1975) Aluminian xanthophyllite and paragonite from Japan. Mineralogical Magazine, 40, 421–423.
Takéuchi, Y. (1966) Structure of brittle micas. Clays and Clay Minerals, 13, 1–25.
Tsipursky, S.I. and Drits, V.A. (1984) The distribution of octahedral cations in the 2:1 layers of dioctahedral smectites studied by oblique-texture electron diffraction. Clay Minerals, 19, 177–193.
Udagawa, S., Urabe, K., and Hasu, H. (1974) The Crystal structure of muscovite dehydroxylate. Japanese Association of Mineralogy, Petrology and Economic Geology, 69, 381–389.
Van Landuyt, J., Tendeloo, G.V., and Amelinckx, S. (1987) Phase Transformations as studied by electron microscopy. Ultramicroscopy, 23, 371–382.
Wardle, R. and Brindley, G.W. (1972) The crystal structures of pyrophyllite, 1*Tc* and of its dehydroxylate. American Mineralogist, 57, 732–750.
Ylagan, R.F., Kim, C.S., Pevear, D.R., and Vrolijk, P.J. (2002) Illite polytype quantification for accurate K-Ar age determination. American Mineralogist, 87, 1536–1545.
Zviagina, B.B., McCarty, D.K., Srodon, J., and Drits, V.A. (2004) Interpretation of infrared spectra of dioctahedral smectites in the region of OH-Stretching vibrations. Clays and Clay Minerals, 52(4), 399–410.

Manuscript received December 17, 2006
Manuscript accepted April 13, 2007
Manuscript handled by Warren Huff